http://eprints.gla.ac.uk/205103/

Deposited on 05 December 2019

Laboratory-Scale Test Platforms for Femto-Satellite Attitude Control Systems

Liviu Stamat[*], Zhongxu Hu[†], Malcolm McRobb[‡] and Colin R. McInnes[§]

University of Glasgow, Glasgow, United Kingdom, G12 8QQ

Femto-satellites have attracted growing attention over the past few years, with various universities taking up the challenge declared by the N-Prize. Many novel designs have been proposed, some of which are equipped with active attitude control based on either magnetic or electro-chromic control systems. However, conventional test platforms are unsuitable for testing control systems on such small length-scales and as such, developing suitable test platforms to be used for testing femto-satellite attitude control algorithms becomes important. This paper proposes six different concepts of laboratory-scale test platforms for femto-satellite attitude control testing, based on various physical laws. These platforms are manufactured using SLA 3D printing technology and then assembled. Qualitative observations are recorded and an experimental setup is devised in order to quantify the total resistive torque that appears in each platform. Results show that two of the designs display a maximum resistive torque on the order of 10^{-6} N m when spinning very rapidly, decreasing to the order of 10^{-7} N m at low angular velocities, which makes these designs suitable for their intended purpose. Finally, future work is proposed towards assessing the suitability of the other four platforms.

Nomenclature

τ	=	torque, N m
k_t	=	torsional constant of a thread
θ	=	angle of displacement, rad
G	=	gravitational constant, Nm^2kg^{-2}
d	=	diameter of a thread, m
l	=	length of a thread, m
I	=	inertia matrix, kgm^2
ω_z	=	Z component of the angular velocity acting on the system, $rads^{-1}$
α_z	=	Z component of the angular acceleration acting on the system, $rads^{-2}$

I. Introduction

Advances in miniaturisation have changed the landscape of the space sector, leading to increased interest in the development of unconventional systems such as femto-satellites (mass less than 100 g) [1]. These devices known as SpaceChips, ChipSats or Satellites-on-a-Chip are now being considered for certain applications deemed unsustainable for CubeSats, such as satellite swarms, global sensor networks and in-orbit damage detection [2–6]. Furthermore, their very small size and mass qualifies them as ideal candidates for being delivered to orbit as secondary piggy-back payloads on larger spacecraft, thus significantly lowering launch cost.

When considering the extremely small length-scale of femto-satellites, a key challenge towards unlocking these applications is the development of an attitude control system, due to the unique interactions between the satellite and the space environment at such small spacecraft sizes [2, 7, 8]. It is shown in [7] how in the context of these length-scales, the individual influences of magnetic interaction, solar radiation pressure (SRP), atmospheric drag and Lorentz forces

---

[*]PhD Student, Division of Systems, Power and Energy, James Watt School of Engineering, l.stamat.1@research.gla.ac.uk.

[†]Research Assistant, Division of Systems, Power and Energy, James Watt School of Engineering.

[‡]Research Assistant, Division of Systems, Power and Energy, James Watt School of Engineering, currently with AAC Clyde Space.

[§]Professor, Division of Systems, Power and Energy, James Watt School of Engineering.

can dominate the effect of gravity on the spacecraft. This could enable novel attitude control strategies based on electro-magnetic control, electro-chromic control [9] or a mix thereof.

However, due to the very same extreme length-scales, the challenge such devices pose extends beyond investigating in-orbit behaviour of potential control strategies. Their extremely small size leads to strict volume and mass constraints for any sensors and actuators that may be implemented. This in turn creates an issue when considering on-ground testing for any proposed control systems, since the torques these miniature actuators can produce are too low to overcome the resistive torques present in most commercially available test platforms, such as conventional air bearings. Laboratory-scale test platforms that are able to accommodate femto-satellite attitude control testing are therefore required.

This paper aims to address this issue by investigating a number of laboratory-scale test platforms for femto-satellite attitude control systems. Proposed concepts are optimized and manufactured using state-of-the-art 3D printing technology. An initial qualitative overview offers insight into the expected performance of each design, then the resistive torques present in each of the test platforms can be measured using a femto-satellite-like Printed Circuit Board (PCB) equipped with an Inertial Measurement Unit (IMU), power and a communication system.

II. Support Systems

ChipSat PCB

The PCB used to test the proposed designs is a prototype ChipSat currently under development which is equipped with an RF communication system and a 10 DoF IMU (accelerometer, gyroscope, magnetometer) [6]. This enables testing of the proposed platforms, since it follows the volume and mass restrictions for a femto-satellite, thus accurately simulating the characteristics of such platforms when in use. The PCB is shown in Fig. 1a and its specifications are provided in Table 1.

Parameter	length	width	minimum height	maximum height	mass
	[*mm*]	[*mm*]	[*mm*]	[*mm*]	[*g*]
PCB	31.36 ± 0.05	31.36 ± 0.05	0.90 ± 0.05		3.11 ± 0.001
PCB MatchBox	33.36 ± 0.05	33.36 ± 0.05	7.50 ± 0.05	10.5 ± 0.05	9.22 ± 0.001

Table 1   PCB MatchBox measurements

MatchBox

In order to avoid solar power dependency, the ChipSat PCB is mounted inside a MatchBox structure that allows the additional space required for a battery. The design of the MatchBox is shown in Fig. 1b and the printed and assembled PCB MatchBox is presented in Fig. 1c. The specifications of the PCB along with the PCB MatchBox assembly are again provided in Table 1. The on-board RF transmitter sends data to a receiver which in turn transmits it via serial connection to a ground station mock-up developed in $MATLAB^{®}$, which parses and records the data stream. A schematic of the experimental setup is provided in Fig. 2.

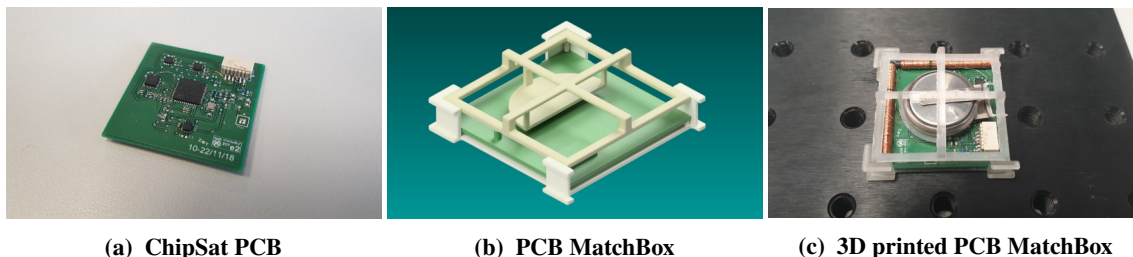| (a) ChipSat PCB | (b) PCB MatchBox | (c) 3D printed PCB MatchBox |

Fig. 1   The sensor PCB with 3D printed MatchBox assembly and setup

The ChipSat PCB used in the scope of this work is also equipped with two custom ferrite-core magnetorquers, as detailed in [6]. These magnetorquers generate a maximum magnetic dipole moment of $0.0025\,\text{Am}^2$. These magnetorquers are used in conjunction with the Helmholtz cage also described in [6], thus being able of generating a maximum torque of order $10^{-6}\,\text{N\,m}$. In Fig. 1c, the magnetorquers are aligned with the X and Y axes of the MatchBox PCB system, with the positive direction of the Z axis going up through the battery.
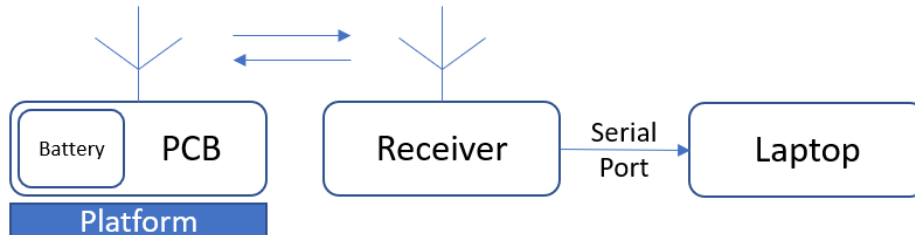

Fig. 2   MatchBox Test Setup

An additional support system is a conventional air bearing supplied by a Bambi® air compressor. The cup of this air bearing, however, weighs 216 g according to the air bearing user manual, which is around 200 times more than the mass of the MatchBox PCB system. This makes it too heavy for the on-board magnetorquers, however the air compressor shall be used in order to test a new platform proposed in the scope of this work, as detailed in III.

III. Proposed Platforms

This section describes the concept and physical analysis for the proposed femto-satellite test platforms. The two key factors that drive the design of each platform are mass and friction. Due to the femto-satellite being extremely low mass and the torque generation capabilities of the actuators being very limited, all designs attempt to minimize test platform mass and friction.

One-axis Suspension Gimbal

The One-axis Suspension Gimbal is essentially a torsional pendulum. The design presented in Fig. 3 is attached to a fixed support by means of a long textile thread. Therefore, the resistive torque τ is the restoring torque that appears in the thread upon deformation, characterized by Eq. (1), where k_t is the torsional constant of the thread and θ is the displacement angle. This relation is the angular form of Hooke's Law [10] and is valid for small values of θ, such that

$$\tau = -k_t\theta \tag{1}$$

An approximation for k_t can be calculated using Eq. (2), with d the diameter of the thread, l its length and G the shear modulus for the material of the thread [10], such that

$$k_t = \frac{\pi G d^4}{32l} \tag{2}$$

Considering that this system is symmetrical around the axis defined by the thread, it can be considered a torsional pendulum. Thus, its rotational motion is described by Eq. (3), with I the moment of inertia of the assembly, such that

$$I\ddot{\theta} = \tau \tag{3}$$

An assumption that drives the performance of this system in the context of femto-satellite attitude control systems is that a longer and thinner thread enables a larger range of angular displacement with minimal resistive torque. This is reflected in Eq. (2), however the validity of this assumption must be experimentally proven.
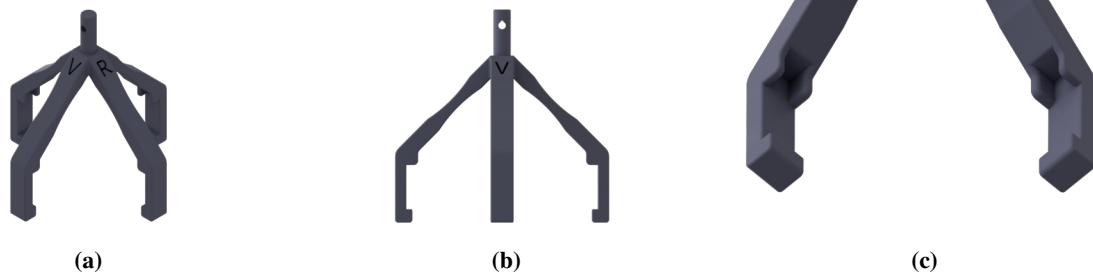
Fig. 3   One-axis Suspension Gimbal Design

Two-axis Suspension Gimbal

The Two-axis Suspension Gimbal is based on the same torsional pendulum concept as its one-axis counterpart, but also employs two radial ball bearings to enable freedom of rotation in one additional axis. A third ball bearing aligned with the suspension thread has the sole purpose of potentially enabling larger angle displacements than in the case of the One-axis Suspension Gimbal, by allowing the system to continue rotating despite the build-up of the resistive torque in the thread. Figure 4 shows the design of this platform, with the ball bearings being the same as the radial bearings described above. The axes of the two bearings are aligned, thus forming one rotational axis, which is orthogonal to the first rotation axis aligned with the thread.
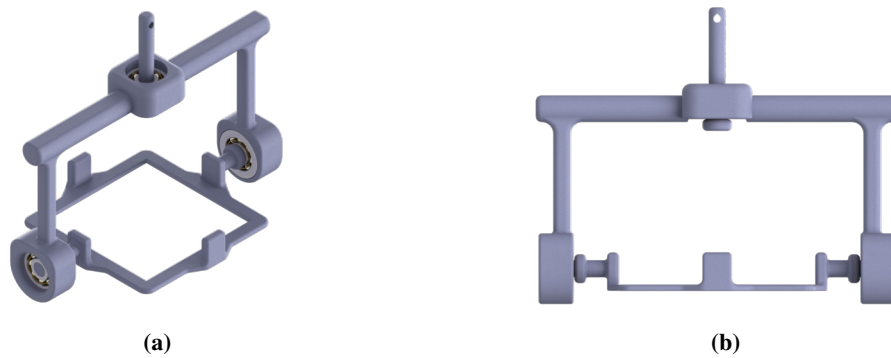

Fig. 4   Two-axis Suspension Gimbal Design

One-axis Ball Bearing Platform

The One-axis Ball Bearing Platform follows the same concept as above, but instead of a thread suspending the system, rotational freedom is enabled by commercial-off-the-shelf ball bearings. Compared to the suspended gimbal, this system is not subject to oscillations induced by angular displacement, however the resistive torque appears due to the friction in the ball bearing. There are two types of friction that need to be quantified in the context of this system - the static friction which must be overcome in order for the system to start moving and the dynamic friction which appears once the system is in motion.

This platform is proposed in two configurations: one using an igus® xiros® xirodur B180 radial deep groove ball bearing, as shown in Fig. 5a and one using an igus® xiros® single row xirodur B180 axial ball bearing, as shown in Fig. 5b. Both components have plastic races with glass ball bearings and their respective sizes are available in Table 2. Figure 5c provides a side view of the design accommodating the radial ball bearing. The interface intended to hold the MatchBox has a longer leg that goes through the ball bearing. This is intended as a design specification in order to lower the centre-of-mass of the system, thus reducing lateral instabilities due to centre-of-mass misalignment.

Type	inner diameter	outer diameter	height
	[*mm*]	[*mm*]	[*mm*]
Radial	3	10	4
Thrust	10	24	9

Table 2   Ball Bearing Specifications

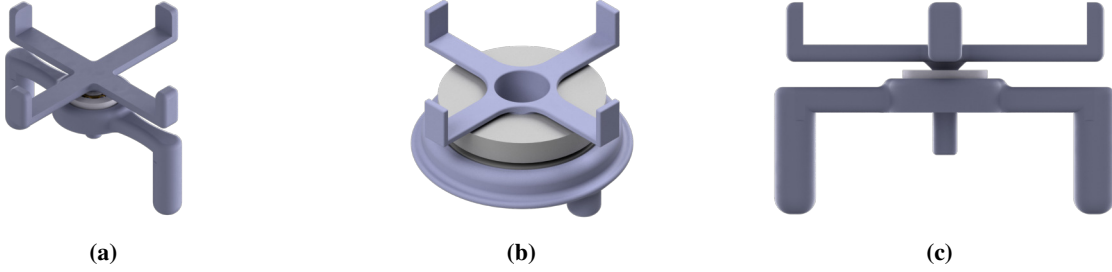(a)   (b)   (c)

Fig. 5   One-axis Ball Bearing Platform Design

One-axis Static Fluid Bearing Platform

The One-axis Static Fluid Bearing Platform follows the same principle as the ball bearing platform described above, with the difference that it employs buoyancy instead of ball bearings. With this approach, a buoyancy force balances gravity acting on the PCB MatchBox, thus enabling freedom of rotation in one axis with minimal friction. Figure 6a shows the design concept for this platform where the fluid tank (white) is fixed on a support surface and the interface to the MatchBox (blue) floats on the surface of the fluid. The MatchBox is attached to an interface point on the bottom of the holder, under the tank, thus keeping the centre-of-mass of the system beneath the centre of pressure, in order to keep the system stable. Figure 6b shows an alternative design which accommodates the MatchBox between four small contact points on the inside. This design is referred to as an open tank static fluid bearing, because it is designed to float on the surface of a fluid, in a arbitrary tank.

Applying an elementary force balance to the holder gives Eq. (4), with m the mass of the holder and MatchBox, g the gravitational acceleration, ρ_f the fluid density and V the volume of fluid displaced, such that

$$mg = \rho_f g V \tag{4}$$

The holder of the first design is shaped to attempt to decrease lateral instability during rotation due to potential misalignments between the centre-of-mass and the rotation axis. In the context of the alternative design, the centre-of-mass must be kept under the centre of pressure of the system to ensure stability, otherwise the holder risks flipping. It is clear that the system must be designed to keep the holder and MatchBox afloat, by adjusting the shape and size of the holder (thus controlling m and V) and by choosing a suitable fluid, thus controlling ρ_f. It is important to note, however, that the choice of fluid is a trade-off, since different fluids will induce different magnitudes of friction with the surface of the holder that must be minimized for the system to perform.
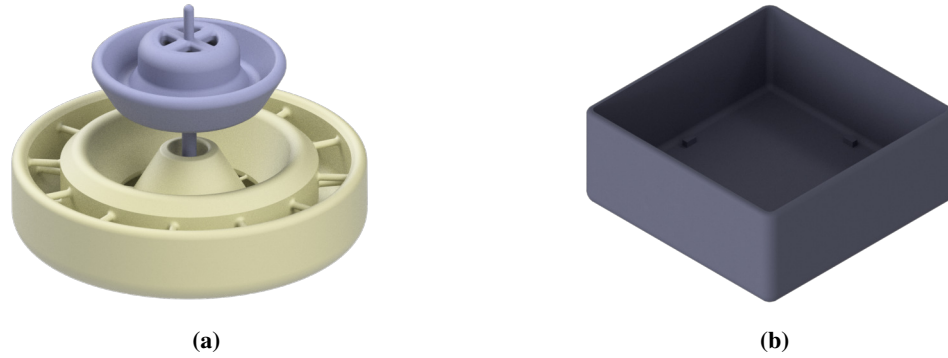
Fig. 6   One-axis Static Fluid Bearing Design

Three-axis Femto-Air Bearing

The Three-axis Femto-Air Bearing is in essence a miniature air bearing driven by two main requirements: to minimize any turbine torques induced by the airflow (due to output hole misalignment) and to minimize the mass and thus the inertia of the interface plate in order to accommodate a femto-satellite. The proposed design for the femto-Air Bearing shown in Fig. 7a is based on the commercial air bearing noted in Section II. It employs eight 1.5 mm diameter output holes placed at a 60° elevation from the bottom of the cup and a 3 mm air inlet aligned with the main rotation axis of the interface. The outlets are positioned at a 45° horizontal separation.

The reason behind aligning the inlet with the main rotation axis is so that any potential turbulent regions of air flow within the bearing are minimized, thus ensuring a smooth flow of air through the bearing cup. Finally, an inverted conical structure is located at the bottom of the cup, on the inside on the bearing system, with the purpose of evenly splitting airflow through all channels within the bearing, thus ensuring an even supply of air to each of the outlets. The design of the interface presented in Fig. 7b is optimized for minimal mass and the empty spherical shape provides space for any additional weights that may be required for centre-of-mass alignment and balancing.

The interface design presented in Fig. 7c is similar to the normal interface design, with the added feature of a balancing plate that enables finer adjustments of the position of the centre-of-mass. Despite this, manually aligning the centre-of-mass with the centre of the spherical interface may prove to be challenging.
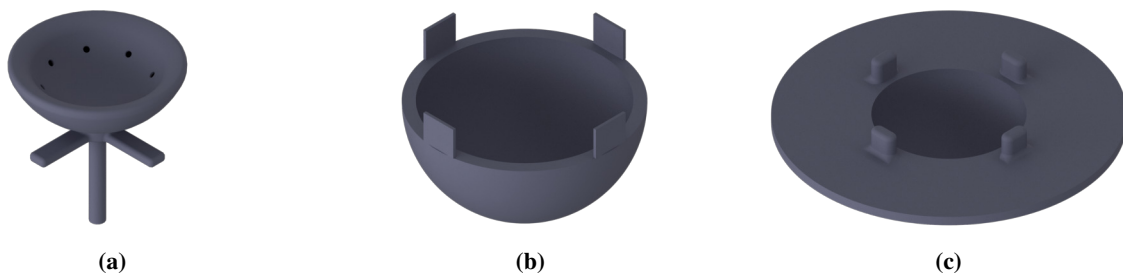

Fig. 7   Three-axis Femto-Air Bearing Design

Three-axis Ring Gimbal

The Three-axis Ring Gimbal is inspired by the three ring gimbal systems used in inertial platforms. In principle, it allows three degree-of-freedom rotation for the femto-satellite. Figure 8 shows the proposed design, which uses the same type of radial ball bearings described above. The key requirement for this platform is that the two bearings for each axis are perfectly aligned, thus eliminating the friction torques that would appear due to bearing axis misalignment. Another key requirement in the interest of avoiding bearing axis misalignment is that the rings are not allowed to bow during manufacture and assembly of the system. Finally, the centre-of-mass of the entire system (including, PCB MatchBox)

must be perfectly aligned with the orthogonal intersection of the three bearing axes, which must also coincide with the locations of the centres of mass for each ring. While the latter is ensured by design, manually aligning the centre-of-mass of the PCB MatchBox with the rest of the system may prove to be challenging.
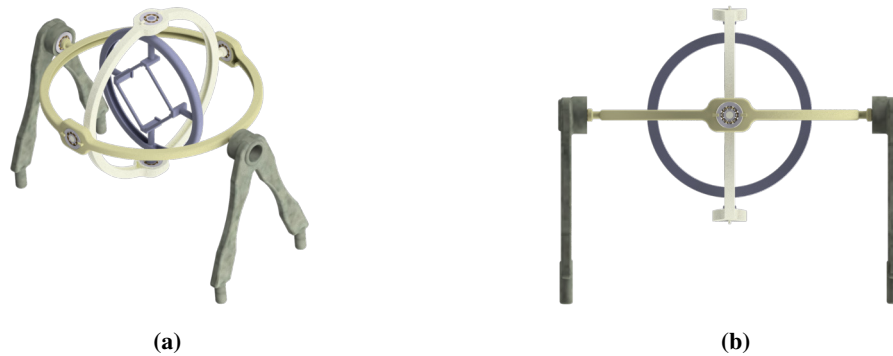

(a)   (b)

Fig. 8   Three-axis Ring Gimbal Design

IV. Manufacture and Testing

The platforms described in Section III have been manufactured using a Formlabs® Form 2® Stereolitography (SLA) 3D printer. The test procedure employed in the context of this work is a spin-up test (SU), aiming to quantify the behaviour of resistive torques in the platform. The procedure for this test is as follows:

- establish data link between ChipSat and Ground Station (GS)
- apply an input torque to the system to start it spinning around one axis
- remove the input torque and record the angular velocity of the system over time
- use angular velocity information provided by the on-board gyroscope to compute the angular acceleration and resistive torques acting on the system.

One-axis Suspension Gimbal (OaSG)

Initial observations regarding the printed components show that the One-axis Suspended Gimbal (Fig. 9) has minimum resistive torque, even after a high number of revolutions (large angle displacement). The SU test conducted on the OaSG supports this observation, as shown in Fig. 10. Here, the system has been spun up in the direction of the positive z-axis, therefore the resistive torque acts on the system in the negative z-axis direction. The plots on the left show data recorded during the entire test and those on the right represent an extract from the same data, after the input torque has been removed.

As shown in Fig. 10, the magnitude of the computed resistive torque is a maximum of 10^{-6}N m recorded under high-spin conditions, which matches the torque generation capabilities of the on-board magnetorquers. For lower angular velocities, the computed resistive torque falls to the order of 10^{-7}N m, which is smaller than the torque generation capabilities of the on-board magnetorquers. This means the OaSG can be further explored as a suitable one-axis femto-satellite test platform, since attitude control tests take place at low angular velocities. An interesting point of this behaviour is the correlation between angular velocity and torque. The plots show a higher resistive torque acting on the system when spinning at a higher angular velocity, which could mean that most of the resistive torque acting on the system is, in fact, due to friction with air, and not due to the thread. If true, this could mean that the resistive torque due to the thread is even smaller in magnitude, thus making the platform even more suitable for femto-satellite attitude control testing. This should be further investigated by running the same type of test inside a vacuum chamber.
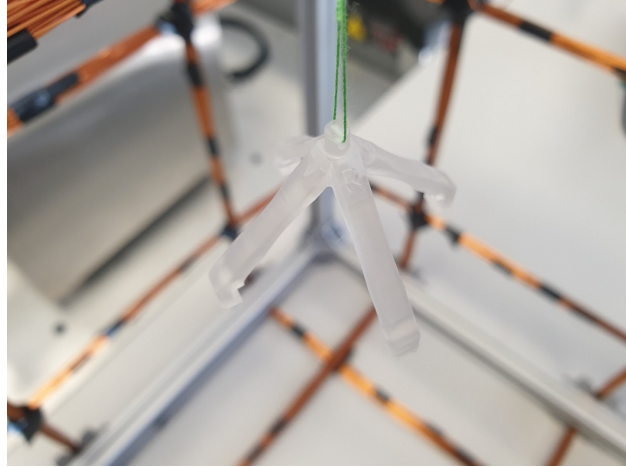
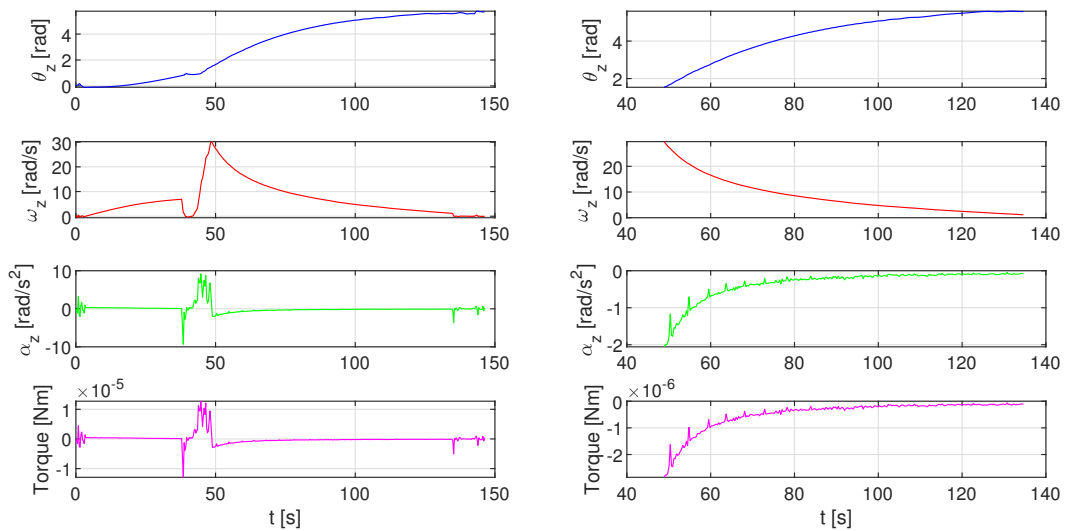**Fig. 9   3D Printed One-axis Suspension Gimbal**

Fig. 10   Angular velocity measured for the OaSG and the corresponding computed angular displacement, angular acceleration and resistive torque.

Two-axis Suspension Gimbal (TaSG)

The Two-axis Suspended Gimbal (Fig. 11) displays two important points. First, even after a large number of revolutions, the horizontal ball bearing still did not begin rotating, which would indicate that the torque induced by the static friction in the bearing is still above the restoring torques building up in the thread as it rotates, which means the ball bearing is redundant and thus not required. This observation is also an indication that the One-axis Ball Bearing Platform may present a higher resistive torque than the suspended gimbals, due to friction in the ball bearing. Secondly, the centre-of-mass of the interface plate and the MatchBox must be centred along the axis of the two bearings, otherwise the bearings become displaced and thus significant added friction is induced.
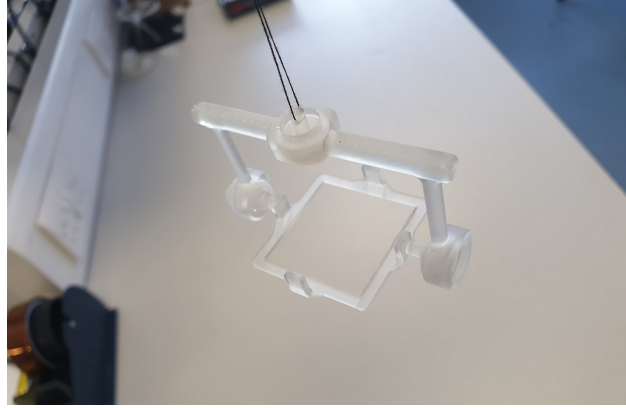
8

Fig. 11   3D Printed Two-axis Suspension Gimbal

Results of a SU test conducted on the main z-axis of the TaSG are shown in Fig. 12. The plots on the left show data recorded during the entire test and those on the right represent an extract from the same data, again after the input torque has been removed. The magnitude of the computed resistive torque is a maximum of 10^{-6}N m recorded under high-spin conditions, which again matches the torque generation capabilities of the on-board magnetorquers. For lower angular velocities, the computed resistive torque falls to the order of 10^{-7}N m, which again is smaller than the torque generation capabilities of the on-board magnetorquers. This means the TaSG can be further explored as a one-axis femto-satellite test platform. These findings are also consistent with the results of the SU test conducted on the OaSG, since both systems are suspended by identical threads. The plots are inverted with respect to those provided in Fig. 10 due to the way the MatchBox PCB interfaces with each platform, thus positive MatchBox z-axis is up for the OaSG and down for the TaSG, while they were both spun up in the same direction. The correlation between torque and angular velocity from the OaSG test results can also be seen in Fig. 12. Thus, the reason the maximum registered torque in the TaSG test is lower than in the OaSG test, despite the TaSG being heavier and wider, can be the fact that the TaSG hasn't reached a similar angular velocity when spinning up and therefore friction effects were lower.
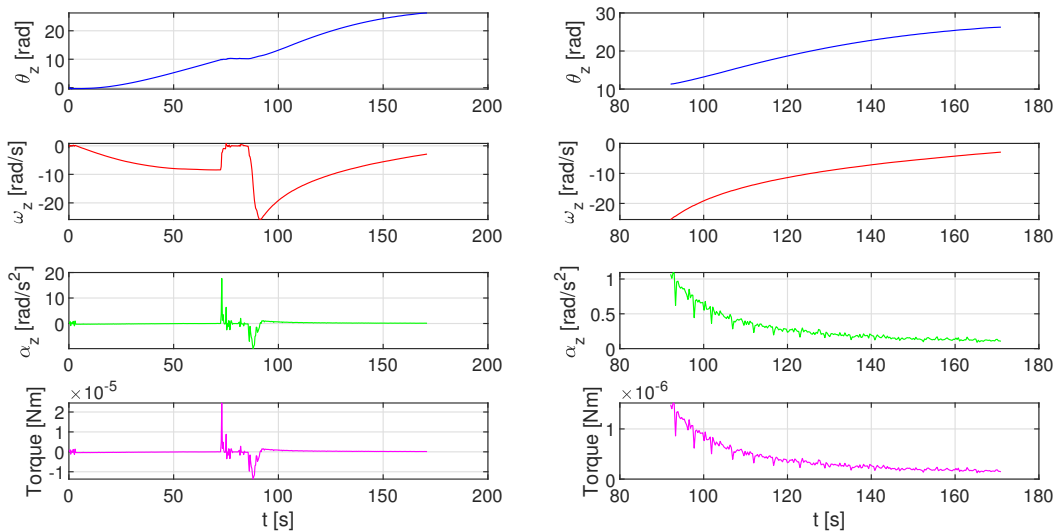

Fig. 12   Angular velocity measured for the main axis (z) of the TaSG and the corresponding computed angular displacement, angular acceleration and resistive torque.

9

One-axis Ball Bearing Platform (OaBBP)

The two One-axis Ball Bearing Platforms (Figs. 13a, 13b) exhibit major differences between the two bearing types, with much more friction being displayed by the axial bearing. These differences are as expected, since the axial (thrust) ball bearing is designed to work better under heavier loads. With the ChipSat being as light as it is, this type of bearing is simply unsuitable within the context of this design. The OaBBP accommodating the radial ball bearing shows good lateral stability and very little susceptibility to centre-of-mass misalignment.
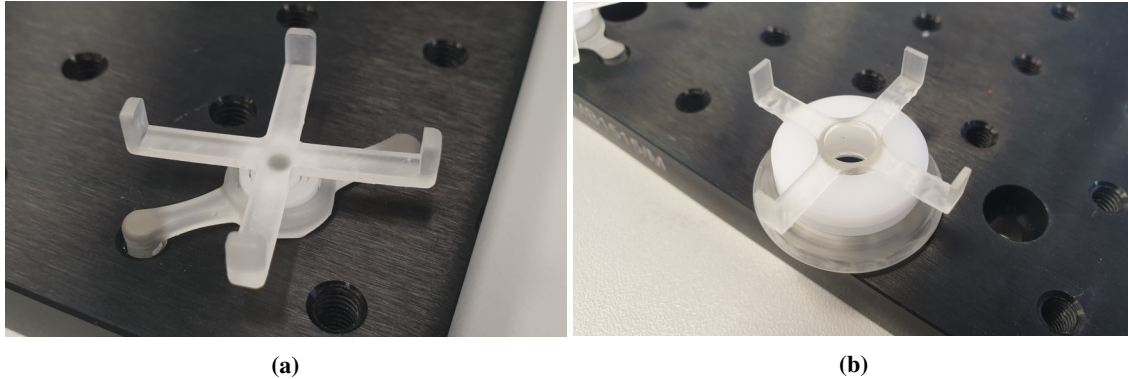

(a)   (b)

Fig. 13   3D One-axis Printed Ball Bearing Platforms

Results of a SU test conducted on the OaBBP are presented in Fig. 14. The plots on the left show data recorded during the entire test and those on the right represent an extract from the same data, after the input torque has been removed. The middle and right-hand-side columns of plots represent the first and second SU tests. These tests are also represented in the left-hand-side column of plots by the angular velocity increasing, then decreasing. The magnitude of the computed resistive torque is 10^{-5} N m, however this is only based on a data pool of seven measurements, due to the ChipSat being restricted by the battery power available. The transmission frequency achieved over the duration of the test is displayed in Fig. 15. This shows a mean achieved frequency of 5.58 Hz, which is not enough to accurately quantify the behaviour of the system over such a short amount of time. As such, these reading are only preliminary and a more suitable power supply must be developed before attempting to accurately quantify the magnitude of the resistive torques acting on the OaBBP.
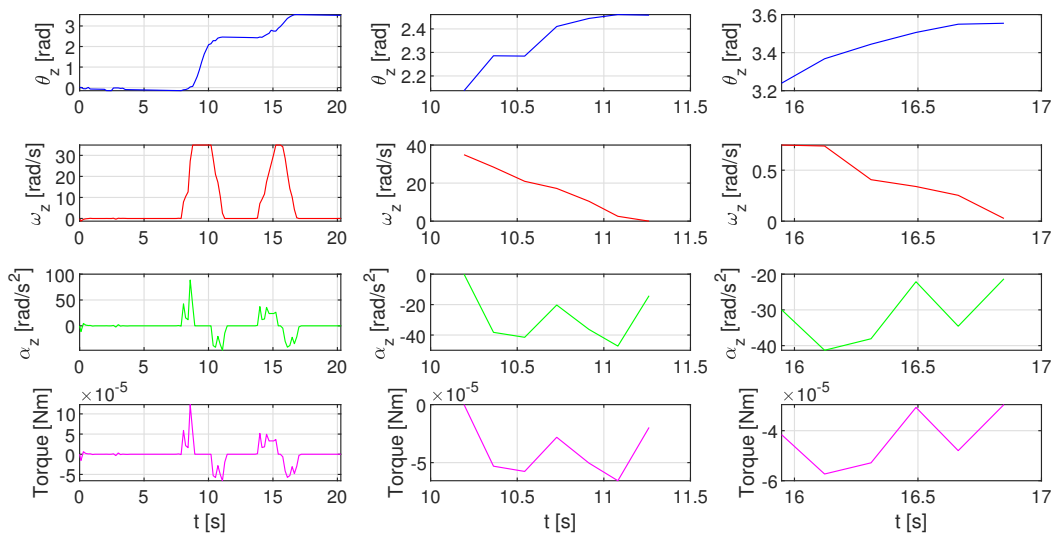

Fig. 14   Angular velocity measured for the main axis (z) of the OaBBP and the corresponding computed angular displacement, angular acceleration and resistive torque.
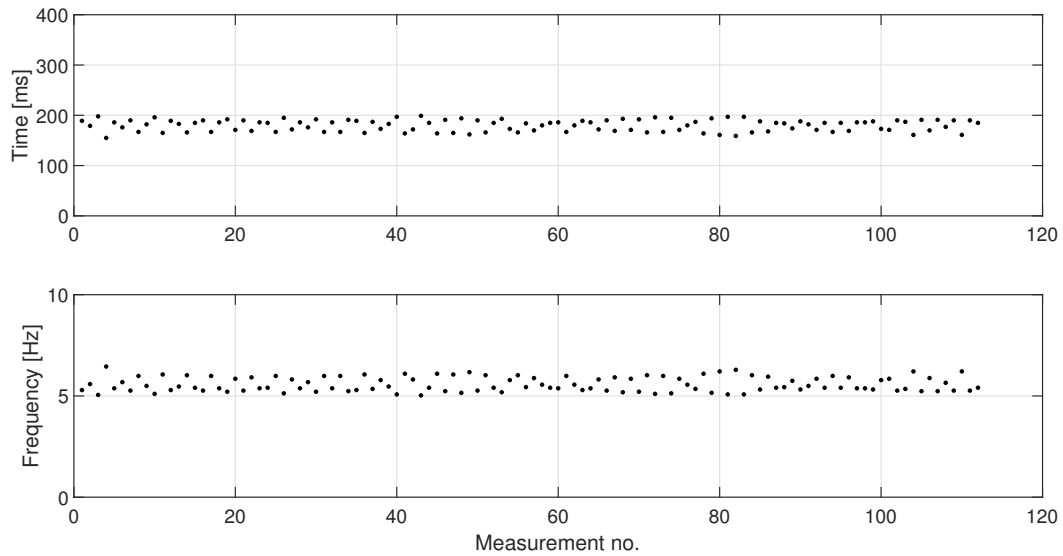
10

Fig. 15   Time and Frequency of Measurements during the SU test for the radial bearing OaBBP

One-axis Static Fluid Bearing Platform (OaSFB)

The main design for the One-axis Static Fluid Bearing Platform displays a major shortcoming. The interface (floater) is too heavy for the volume of water that it can displace in the tank channel and as such does not float as expected. The alternative design, however, floats successfully and is stable against lateral movements on the surface of the fluid (in this case, water). Furthermore, manufacturing this design requires a very limited amount of material and post-print processing, thus making this platform potentially the easiest and cheapest to manufacture. However, qualitative observations suggest a higher resistive torque present in the water-resin contact surface as opposed to the resistive torque displayed by the OaSG and TaSG. This observation is also supported by the fact that water is a much more viscous fluid than air.
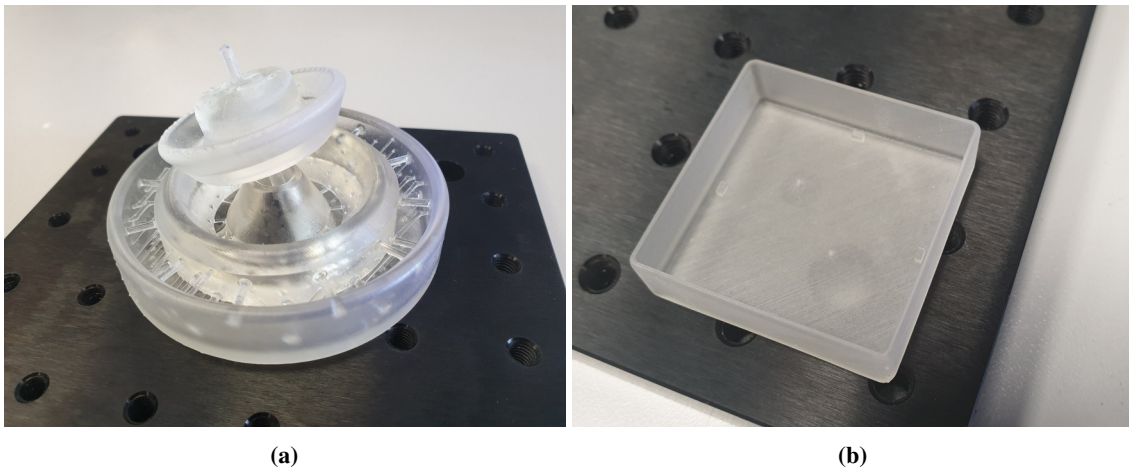

(a)   (b)

Fig. 16   3D Printed One-axis Static Fluid Bearing

11

Three-axis Femto-Air Bearing (TafAB)

The Three-axis Femto-Air Bearing (Fig. 17) is a promising platform. While easily one of the most complex of the proposed designs, qualitative observations show a very stable interface (applicable to both interface designs) with little to no induced torque and an extremely low mass. Clearly, mounting the MatchBox on the interface comes with a shift in the centre-of-mass, which in this case must be aligned with the centre of the supporting sphere. Therefore, centre-of-mass adjustments are required. Attempting to fulfil this requirement manually has proven very challenging, even when using the interface with the extended balancing plate, since the design is based on an air bed and thus extremely susceptible to minimal centre-of-mass misalignment in either axis. A new approach to balancing the system must be considered, by finding the centre-of-mass of the ChipSat PCB and then designing the MatchBox to compensate for it, thus creating a MatchBox PCB system with the centre-of-mass in the middle. This would make it easier to interface with the TafAB interface, since it would only require manually shifting the centre-of-mass of the MatchBox-interface system vertically.
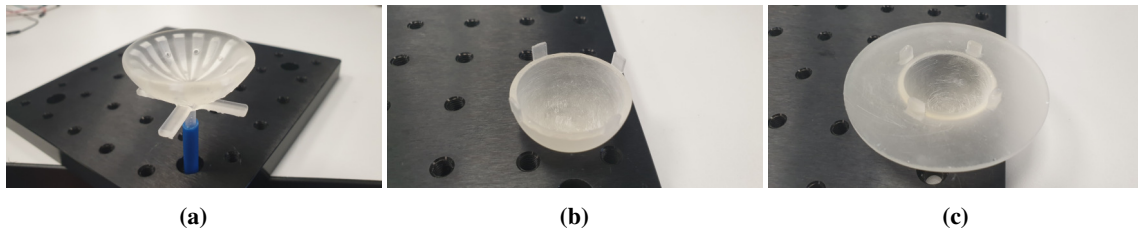

(a)   (b)   (c)

Fig. 17   3D Printed Three-axis Femto-Air Bearing

Three-axis Ring Gimbal (TaRG)

The Three-axis Ring Gimbal (Fig. 18) displays low overall friction induced by the bearings, however it presents two key design issues that need to be addressed. First, as with the Two-axis Suspended Gimbal, the centre-of-mass of the MatchBox must be accurately aligned with the centre-of-mass of the three rings, which in turn must be aligned with the point of orthogonal intersection of the three rotation axes of the ball bearings. While the latter is enabled by design, achieving the former has proven very challenging and as such a more accurate way of ensuring alignment is required. As in the case of the TafAB, the MatchBox PCB system must first be mass-centred. This would then require the centre-of-mass to only be manually shifted along one axis in order to align it with the centre of the ring system.
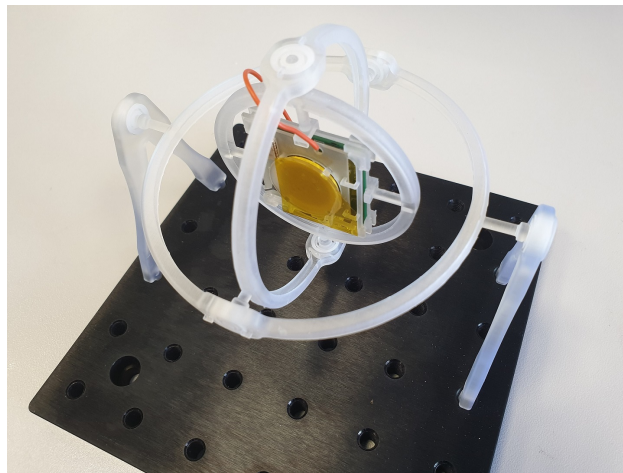

Fig. 18   3D Printed Three-axis Ring gimbal

Manufacturing requirements

Table 3 lists all required resin volumes for each individual component of each platform discussed. Furthermore, the material costs for each component is shown in Fig. 19. Considering these manufacturing prices are all under 2£per component, the production of these test platforms is extremely affordable. This enables:

- further investigation of the platforms with the goal of qualifying them as fully-fledged test platforms for femto-satellite systems
- easier access to femto-satellite attitude control testing, due to the very affordable nature of manufacturing one of these platforms.

Platform	Part	Model [ml]	Print supports [ml]	Total [ml]	Material cost [£]
MatchBox	Cradle	0.57	2.21	2.78	0.33
	Cover	0.50	2.76	3.26	0.39
One-axis Suspended Gimbal	Main	1.35	1.48	2.83	0.34
One-axis Ball Bearing Platform (radial)	Cradle	0.46	1.12	1.58	0.19
	Interface	0.25	1.59	1.84	0.22
One-axis Ball Bearing Platform (thrust)	Cradle	1.06	1.30	2.36	0.28
	Interface	0.77	1.90	2.67	0.32
One-axis Static Fluid Bearing	Tank	11.11	4.49	15.60	1.87
	Interface	1.93	2.27	4.20	0.50
	Alt. Interface	4.75	3.35	8.10	0.97
Two-axis Suspended Gimbal	Main	2.28	3.69	5.97	0.72
	Thread Pin	0.16	0.23	0.39	0.05
	Interface	0.81	2.81	3.62	0.43
Three-axis Femto-Air Bearing	Cup	6.53	5.75	12.28	1.47
	Interface	3.58	3.54	7.12	0.86
	Interface Plate	9.91	6.71	16.62	1.20
Three-axis Ring Gimbal	Inner ring	2.26	8.39	10.65	1.28
	Middle ring	2.41	10.58	12.99	1.56
	Outer ring	2.90	10.07	12.97	1.56
	Leg (x2)	5.36	3.30	17.32	1.04

Table 3   Material requirements per printed component according to Formlabs firmware
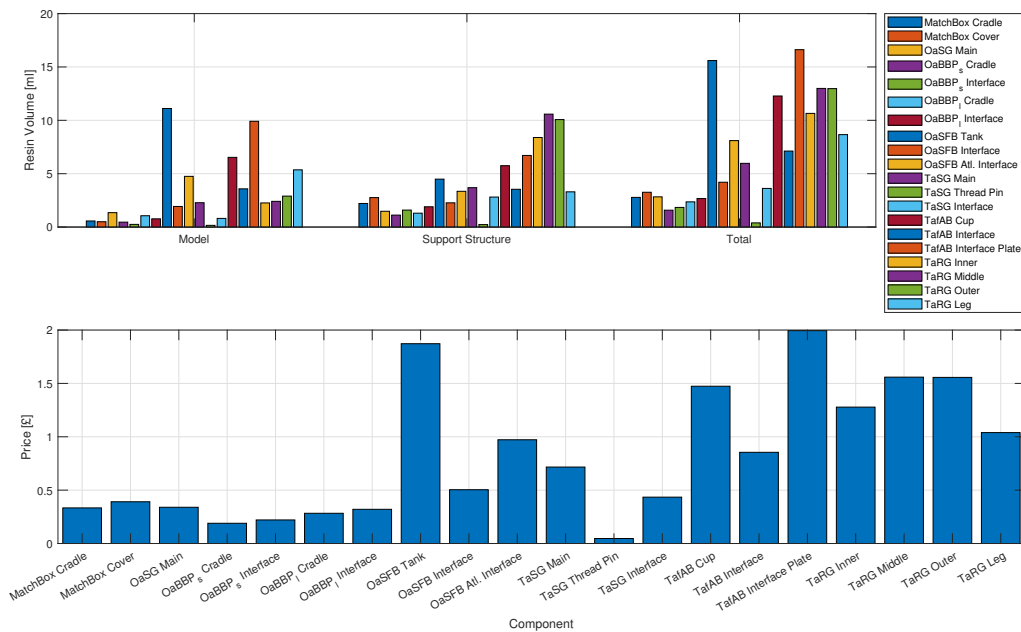
Fig. 19   Resin Volume for each printed component and cost thereof

V. Recommendations

As discussed in Section IV, the resistive torque registered for the OaSG in a high-spinning configuration matches the torque generation capabilities of the magnetorquer system on board the MatchBox PCB. Results also show its resistive torque being much lower for slow slew-type manoeuvres. Therefore, this design is suitable and the next step should be to more accurately quantify its resistive torque for slow manoeuvres at small displacement angles. This resistive torque can then be used as part of future simulations for attitude control algorithms.

The results of the TaSG also prove its suitability as a one-axis test platform, however the ball bearing aligned with the thread axis has proven to be redundant and as such can be removed from the design. Afterwards, the system should also be characterized in terms of its resistive torque, in order for it to be qualified and considered for future simulations. For the secondary axis, however, a higher data rate must be achieved on the MatchBox PCB, since testing it would otherwise face the same issues as the One-axis Ball Bearing Platform. These two systems stop rotating soon after removing the input torque and as such a 5.58Hz data rate will not suffice in order to accurately determine the resistive torques generated by the ball bearings. The fact that these platform stop rotating quickly in the absence of the input torque also suggests a high resistive torque, however experimentally quantifying this resistive torque may still be worthwhile.

As noted in Section IV, the initial OaSFB design is not successful due to the interface being to heavy to stay afloat. The secondary design, however, successfully floats and as such should be tested with the on-board magnetorquers and the Helmholtz coil system in order to assess its suitability as a femto-satellite test platform. The resistive torques displayed however, should be expected to be higher than in the case of the previous three systems, due to the viscous nature of water as opposed to air.

The TafAB is a promising platform, however mass balancing it proves very difficult when done manually. As such, the next step should be to restructure the Matchbox in order for the MatchBox PCB system to be mass balanced when stand-alone. This would then allow for a much easier balancing of the centre-of-mass when the MatchBox PCB is mounted on the TafAB interface, because the only shift required in the centre-of-mass of the MatchBox-interface system would be downwards and the interface is already designed to accommodate weights specifically for that purpose. This would then enable the TafAB to be experimentally tested. Based on qualitative observations thus far, this platform is expected to also be suitable as a femto-satellite attitude control test platform, however this observation must be supported by numerical tests.

14

As in the case of the TafAB, mass balancing the TaRG has proven difficult. Once a new mass-balanced MatchBox PCB is manufactured, this should become easier for the same reasons stated previously. The TaRG, however, is a complex system and experimentally testing it is challenging. The first step, however, would be to test it using the on-board magnetorquers in conjunction with the Helmholtz coil system in order to asses whether this platform may be suitable as a test platform for femto-satellites.

VI. Conclusions

This paper has proposed six laboratory-scale femto-satellite attitude control test platforms which have been manufactured and assembled using SLA 3D printing technology. Designing test platforms for femto-satellite length-scales has proven to be challenging due to the constraints posed by the ChipSat PCB, such as very limited power and torque generation capabilities. However, some of the proposed designs have been successfully tested and results show promise within the scope of qualifying these platforms as future femto-satellite attitude control test platforms. Future work aims to further investigate the platforms that have been successfully tested and correct the issues that have arisen when attempting to test the rest of the proposed designs.

However, while designing these platform is challenging, the costs of manufacturing and assembling them have proven to be minimal. This invites further work on the topic, allowing for easy access to the technologies in the scope of further testing. Furthermore, the low costs of manufacturing one of these designs goes hand-in-hand with part of the motivation for femto-satellite as the next step in space miniaturisation, since the costs of both the satellites and the testing platforms required is very low, thus enabling cheaper access to space.

VII. Acknowledgements

References

[1] Perez, T. R., and Subbarao, K., "A survey of current femtosatellite designs , technologies , and mission concepts," *Journal of Small Satellites*, Vol. 5, No. 2, 2016, pp. 467–482. URL `http://www.jossonline.com/wp-content/uploads/2016/10/Perez-Final-A-Survey-of-Current-Femtosatellite-Designs-Technologies-and-Mission-Concepts1.pdf`.

[2] McInnes, C. R., Ceriotti, M., Colombo, C., Sanchez Cuartielles, J.-P., Bewick, R., Heiligers, J., and Lücking, C., "Micro-to-Macro: Astrodynamics at Extremes of Length-scale," *Acta Futura*, Vol. 4, 2011, pp. 81–97. https://doi.org/10.2420/AF04.2011.81, URL http://strathprints.strath.ac.uk/33785/.

[3] Barnhart, D. J., Vladimirova, T., and Sweeting, M. N., "Very-Small-Satellite Design for Distributed Space Missions," *Journal of Spacecraft and Rockets*, Vol. 44, No. 6, 2007, pp. 1294–1306. https://doi.org/10.2514/1.28678, URL http://arc.aiaa.org/doi/10.2514/1.28678.

[4] Barnhart, D. J., Vladimirova, T., Baker, A. M., and Sweeting, M. N., "A low-cost femtosatellite to enable distributed space missions," *Acta Astronautica*, Vol. 64, 2009, pp. 1123–1143. https://doi.org/10.1016/j.actaastro.2009.01.025.

[5] Manchester, Z., Peck, M., and Filo, A., "KickSat : A Crowd-Funded Mission To Demonstrate The World's Smallest Spacecraft," *Annual AIAA/USU Conference on Small Satellites*, 2013, pp. SSC13–IX–5.

[6] Hu, Z., Timmons, T., Stamat, L., and McInnes, C., "Development of a 10g Femto-Satellite with Active Attitude Control," *Reinventing Space 2019*, Belfast, 12-14 November 2019.

[7] Atchison, J. A., and Peck, M. A., "Length Scaling in Spacecraft Dynamics," *Journal of Guidance, Control, and Dynamics*, Vol. 34, No. 1, 2011, pp. 231–246. https://doi.org/doi:10.2514/1.49383.

[8] Colombo, C., Lücking, C., and McLnnes, C. R., "Orbital dynamics of high area-to-mass ratio spacecraft with J2 and solar radiation pressure for novel Earth observation and communication services," *Acta Astronautica*, Vol. 81, No. 1, 2012, pp. 137–150. https://doi.org/10.1016/j.actaastro.2012.07.009.

[9] Colombo, C., Lücking, C., and McInnes, C. R., "Orbit evolution, maintenance and disposal of SpaceChip swarms through electro-chromic control," *Acta Astronautica*, Vol. 82, No. 1, 2013, pp. 25–37. https://doi.org/10.1016/j.actaastro.2012.05.035.

[10] Mohazzabi, P., and Shefchik, B. M., "A universal relationship between spring constant and torsion constant," *Journal of Physics and Chemistry of Solids*, Vol. 62, 2001, pp. 677–681. https://doi.org/10.1016/S0022-3697(00)00205-5.